A&A 487, 323–327 (2008)
DOI: 10.1051/0004-6361:200809935

Astronomy & Astrophysics

Long-term monitoring of θ^1 Ori C: the spectroscopic orbit and an improved rotational period★ *(Research Note)*

O. Stahl[1], G. Wade[2], V. Petit[3], B. Stober[4], and L. Schanne[5]

[1] ZAH, Landessternwarte Königstuhl, 69117 Heidelberg, Germany
e-mail: O.Stahl@lsw.uni-heidelberg.de
[2] Dept. of Physics, Royal Military College of Canada, PO Box 17000, Station Forces, Kingston, ON, K7K 7B4, Canada
[3] Département de physique, génie physique et optique, Centre de recherche en astrophysique du Québec, Université Laval, Québec (QC) G1K 7P4, Canada
[4] Nelkenweg 14, 66791 Glan-Münchweiler, Germany
[5] Hohlstraße 19, 66333 Völklingen-Ludweiler, Germany

Received 9 April 2008 / Accepted 12 June 2008

ABSTRACT

Context. The young O-type star θ^1 Ori C, the brightest star of the Trapezium cluster in Orion, is one of only two known magnetic rotators among the O stars. However, not all spectroscopic variations of this star can be explained by the magnetic rotator model. We present results from a long-term monitoring to study these unexplained variations and to improve the stellar rotational period.
Aims. We want to study long-term trends of the radial velocity of θ^1 Ori C, to search for unusual changes, to improve the established rotational period and to check for possible period changes.
Methods. We combine a large set of published spectroscopic data with new observations and analyze the spectra in a homogeneous way. We study the radial velocity from selected photo-spheric lines and determine the equivalent width of the Hα and He II λ4686 lines.
Results. We find evidence for a secular change of the radial velocity of θ^1 Ori C that is consistent with the published interferometric orbit. We refine the rotational period of θ^1 Ori C and discuss the possibility of detecting period changes in the near future.

Key words. stars: individual: θ^1 Ori C – stars: emission-line, Be – stars: variables: general – stars: circumstellar matter – stars: early-type

1. Introduction

The young O star θ^1 Ori C, the brightest star of the Trapezium cluster in Orion, is one of the only two O-type stars with detected magnetic fields (the other is HD 191612, cf. Donati et al. 2006). Regular variations of the Hα line with a period of 15.4 days were discovered from equivalent width measurements by Stahl et al. (1993). Later, this same period was also detected in e.g. UV spectral lines (Walborn & Nichols 1994) and the X-ray flux (Gagné et al. 1997).

The magnetic field of θ^1 Ori C, which also varies according to the 15.4 day period, was first detected by Donati et al. (2002) and later studied in more detail by Wade et al. (2006). For a detailed spectroscopic analysis of the star see Simón-Díaz et al. (2006).

The observations are explained conceptually by the magnetically-confined wind shock (MCWS) model, originally proposed by Babel & Montmerle (1997). In this model, a dipolar magnetic field confines the outflowing radiatively-driven stellar wind, which is channeled toward the magnetic equator where it generates a strong shock. The resulting circumstellar plasma is forced to rotate with the star, generating periodic variability of the emitted optical, UV and X-ray fluxes. This model has more recently been extended using MHD simulations by ud-Doula & Owocki (2002) and Gagné et al. (2005), who have investigated the stability and dynamics of this phenomenon.

The period of θ^1 Ori C was determined to be 15.422 ± 0.002 days by Stahl et al. (1996) and later revised to 15.426 ± 0.002 by Stahl (1997). However, most publications (e.g. Wade et al. 2006) use the older period value of 15.422 days. The difference in both periods has now accumulated to a phase difference of about 0.1, which is quite significant. Observations obtained at the current epoch should therefore be able to distinguish between these two periods.

In addition to the strict periodicity, θ^1 Ori C also shows additional variations, which are probably not periodic, or have unknown periods e.g. the spectral type variations reported by Walborn (1981) or the radial velocity variations found by Stahl et al. (1996). Also, θ^1 Ori C is in fact a multiple system and interferometric measurements recently propose a long orbital period of more than ten years (Kraus et al. 2007; Patience et al. 2008).

The published radial-velocity measurements have been analyzed by Vitrichenko (2002), but more data are available.

Long-term monitoring is necessary to study these variations. We therefore collected all available published spectra of θ^1 Ori C and obtained new observations to study long-term trends, to search for unusual variations and to improve the determination of the rotational period.

★ Tables 4 and 5 are only available in electronic form at http://www.aanda.org

2. Observations

For the study of the long-term variations, we primarily used published echelle observations: the Heros data published by Stahl (1997), complemented by a few other observations obtained with the same instrument; the Feros observations published by Reiners et al. (2000); the MuSiCoS spectra published by Wade et al. (2006); a few ESPaDOnS spectra (Petit et al. 2008) and two spectra extracted from the Elodie archive (Moultaka et al. 2004, `http://atlas.obs-hp.fr/elodie/`). All of these observations cover a large spectral range with high resolving power.

In addition, we have been obtained a few spectra with amateur instruments. For these observations we used the spectrograph Lhires III, which is available from `http://www.shelyak.com/`, attached to Celestron 14″ Schmidt-Cassegrain telescopes at private observatories. The detector for most observations was a CCD with 2184×1472 pixels (used with 2×2 binning) with a pixel size of 6.8 μm. A grating with 1200 lines/mm was used for most observations (Lhires III, 1), resulting in a spectral resolution of about 1.0 Å. A few spectra were obtained with a grating with 2400 lines/mm, resulting in a higher resolution of 0.5 Å (Lhires III, 2). One spectrum was obtained with the 2400 lines/mm grating, but with another detector with 1536×1024 pixels with 9 μ pixel size (Lhires III, 3). All of these spectra were reduced with ESO-Midas, using standard procedures. The wavelength calibration was performed using a Neon lamp. The spectra of θ^1 Ori C show strong nebular lines from the Orion nebula. These lines were used to verify the wavelength solution. The Lhires observations cover a relatively small spectral range around Hα and were used only for the equivalent width determination of Hα. A summary of the data used is given in Table 1.

3. Radial velocity variations

The radial velocity variations of θ^1 Ori C have been studied by various authors (e.g., Vitrichenko 2002), but with ambiguous results. It appears likely that the variations reflect the 15.4 day rotational modulation, as well as mysterious, shorter- and longer-term variations. However, the published radial velocities show significant scatter. In light of the interferometric orbits published by Kraus et al. (2007) and Patience et al. (2008) with a period of more than ten years, a re-analysis of the radial velocities seems warranted. As most spectral lines vary significantly with the 15.4 day period, we decided to use only the C IV line doublet at $\lambda\lambda$5801.51, 5812.14 Å, the He II λ5411.424 line and the O III λ5592.37 line for radial velocity studies. These lines seem to be more weakly affected by the rotational modulation (Stahl et al. 1996) and as a group they provide consistent results. The lines were modeled by fitting Gaussians to the line profiles, which matches the lines very well. The result is reported in Table 4 and plotted for the C IV lines in Fig. 1. A closer analysis shows small, but significant systematic offsets of the order of a 2–3 km s^{-1} between different lines. These offsets are probably due to blends or atmospheric stratification. All lines show the same variability pattern, however.

As can been seen in Fig. 1, a large scatter on short time scales is obvious. These variations have already been detected by Stahl et al. (1993). The scatter is partly due to variations with the rotational period, but primarily it is caused by occasional variations on other timescales (cf. Fig. 2). From Fig. 2, a period of about 60 days seems possible. However, a period analysis of the radial velocities does not show a significant peak near this period. In the period range below 100 days, only the 15.4 day period is significant in the radial-velocity data. Therefore, the rapid

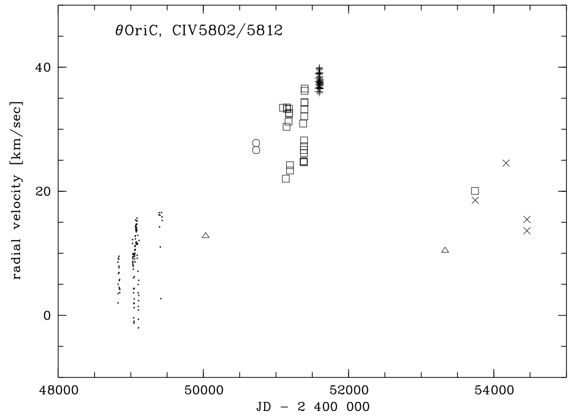

Fig. 1. Radial velocity of C IV $\lambda\lambda$5801, 5812 versus Julian Date. The symbols denote different instruments. •: Flash, ○: Heros, □: Feros, △: Elodie, +: Musicos, ×: Espandons.

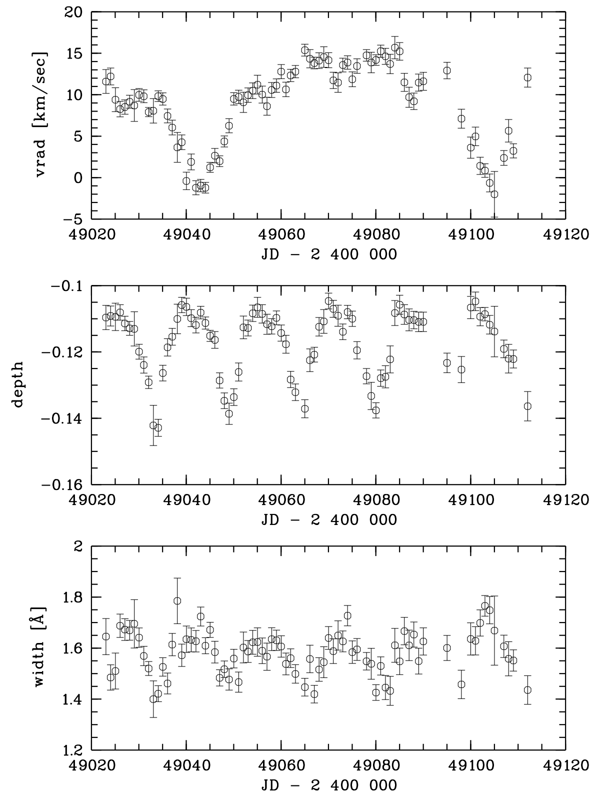

Fig. 2. Average radial velocity, line depth and FWHM, together with the 1σ error bars, of the C IVλ5801, 5812 lines for part of the time covered. The radial velocity shows strong variations, but not with the 15.4 d period. The line depth and width are clearly variable with the 15.4 d period.

variations in radial velocity are probably not periodic, and we speculate that they may be due to (stellar) atmospheric effects.

The Gaussian fit to the line also measures the line width (FWHM) and depth of the lines. Both quantities are strongly variable on short timescales (by about ±30%), but without any obvious long-term trend. In contrast to the radial velocities, the variations in width and depth are mostly due to rotational modulation (cf. Fig. 2). The width of the lines and their depth are clearly correlated. The lines are deeper when they are narrower, see Fig. 3. The equivalent widths are therefore less variable, by only about ±10%.

Table 1. Summary of instrumentation used for this study. Most of the spectra (except the Lhires spectra, have been partly published. The signal-to-noise ratio for the echelle data is strongly dependent on wavelength, but above 100 in the spectral ranges used for most of the spectra.

Instrument	Resolution [$\lambda/\Delta\lambda$]	Wavelength range [Å]	JD - 2 400 000
Flash	20 000	4000–6800	48 822–49 333
Heros	20 000	3450–5700, 5800–8625	49 759–50 727
Feros	48 000	3700–9200	51 097–51 394, 53 740
Elodie	42 000	4000–6800	50 030, 53 329
Musicos	35 000	4480–6620	51 577–51 608
Espadons	65 000	3690–10 485	53 744, 54 169, 54 456–54 457
Lhires III,1	6000	6350–6900	54 505–54 521
Lhires III,2	12 000	6500–6700	54 527–54 544
Lhires III,3	12 000	6500–6700	54 505

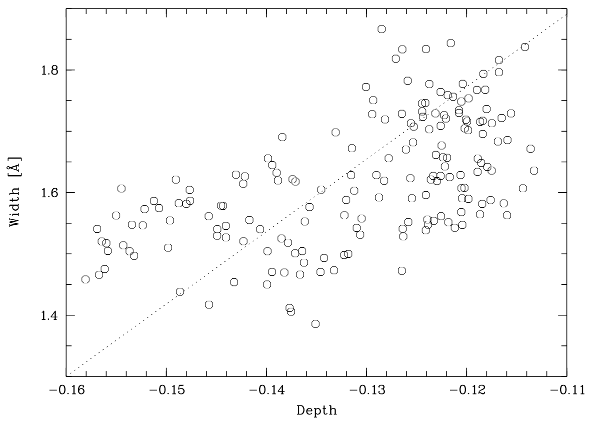

Fig. 3. Correlation of FWHM and line depth of C IVλ5801, 5812.

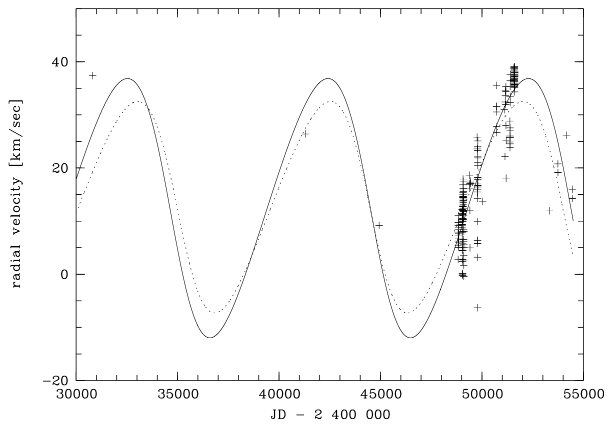

Fig. 4. Heliocentric radial velocity versus Julian date. The dashed line represents an orbital solution based on the parameters published by Patience et al. (2008), with only the systemic velocity γ as a free parameter. The full line represents a solution which is within the errors compatible with interferometric orbit, but fits the radial velocities better.

In Fig. 1, a large increase in radial velocity between 1992 and 1999 is obvious, followed by lower velocities after 2004. If these changes are due to movement in a binary system, the data suggest a long-period orbit.

In order to improve the time coverage, we searched for older published radial velocities. A number of authors have measured the radial velocity of θ^1 Ori C. These measurements have been summarized by Vitrichenko (2002). However, their Table 1 contains errors in the mean time of the observations and partly averages data obtained over several seasons. The data of Abt et al. (1991) have been obtained over many years and are based only on the Balmer lines (which are in strong emission, and highly variable). The same is true for the data of Frost et al. (1926). The average data reported by Vitrichenko (2002) for both data sets are averaged over many seasons and therefore not useful for our period study. Therefore, only the data in Table 2 remain. They are averages over relatively short intervals and give reliable radial velocities.

A possible orbital origin for the trend in the radial velocity was already discussed by Donati et al. (2002) and Kraus et al. (2007), but we now cover a substantially longer time interval. However, our data alone still do not allow us to determine an unambiguous period. An interferometric orbit was recently published by Kraus et al. (2007), and more recently revised with newer data by Patience et al. (2008). If we assume that the radial velocity variations result from the orbit published by Patience et al. (2008), we can fit an orbital solution.

In Fig. 4, the radial velocity (mean of all lines in Table 4 and the values from Table 2) is plotted versus Julian date. All parameters derived from the interferometric orbit of Patience et al. (2008) have been kept fixed. We derived the K value of the orbit from the relation $K = (2\pi/P)a\sin i/\sqrt{1-e^2}$, using the

Table 2. Published radial velocities. "n" is the number of spectra used.

Reference	JD - 2 400 000	rad. vel	n
Struve & Titus (1944)	30 813	37.4	14
Conti (1972)	41 302	26.4	10
Morrell & Levato (1991)	44 932	9.2	6

parameters of Patience et al. (2008) and a distance of 440 pc (Jeffries 2007). The only free parameter was the systemic velocity γ (dashed line). It can be seen that the radial velocity data are compatible with the interferometric orbital parameters. If we optimize the radial-velocity solution by varying all parameters, starting with the interferometric parameters, we obtain another solution plotted in Fig. 4 (full line). Both solutions are summarized in Table 3.

Note that our solution is not unique. Within the errors given by Patience et al. (2008) several different radial velocity solutions of similar quality are possible. Good solutions are also possible with parameters which are incompatible with the interferometric orbit. Therefore it is not possibly to give a reliable error estimate for our solution. This is due to our very incomplete phase coverage and the large short-term scatter. Both effects prevent a unique solution with the available data. However, the period P and the system velocity γ are relatively robust.

Solutions with about half the period are also possible. In particular, a highly eccentric orbit with a period near 11 years, similar to the one proposed by Kraus et al. (2007), fits the data reasonably well, although not with the phases given by

Table 3. Summary of orbital parameters. Note that the radial velocity solution is not unique. The given solution is close to the parameters of Patience et al. (2008).

Orbit	P (days)	T_0 (JD)	ω (deg)	ε	K	γ
Patience et al. (2008)	9497 ± 1461	2 425 610 ± 2154	96.9 ± 118.7	0.16 ± 0.14	19.9	13 ± 3
radial velocity solution	9880	2 424 932	99.3	0.142	24.4	13

Kraus et al. (2007) and with larger deviations than the solution presented above. Such a short period seems to be excluded by the interferometric data published by Patience et al. (2008), however. Clearly, a longer time coverage is needed to derive a more reliable solution.

4. Equivalent width variations of Hα and He II λ4686

The equivalent width of the Hα line of θ^1 Ori C shows periodic variations, corresponding to the 15.4 day rotation period of the star (Stahl et al. 1993). We measured the equivalent width after subtraction of the nebular lines, following the procedure described by Stahl et al. (1996). The line was integrated between 6545 and 6580 Å. The equivalent widths are listed in Table 5. For completeness, we also include the measured equivalent widths of HeII λ4686 in the table. The subtraction of the nebular lines is subjective and introduces an error, which is difficult to quantify. The error is small for the data with the highest resolution, but increases with decreasing resolution. We combined our new results with the published results to improve the period. From the AOV method (Schwarzenberg-Czerny 1989) we derive a best period of 15.424 ± 0.001 days. The phase diagram obtained with this period is shown in Fig. 5. The new period is, within the error bars, in agreement with all published values, also with the value originally obtained by Stahl et al. (1996) from IUE observations.

The error in the period is smaller than that obtained from previous studies. However, because θ^1 Ori C is a member of a binary, the times need to be corrected for light-travel effects due to orbital motion. Because of the uncertain orbit, this correction has not yet been applied.

As can be seen in Fig. 5, the new measurements fit very well in the phase diagram, although the scatter is larger than with the higher resolution echelle data. This demonstrates that the magneto-spheric emission of θ^1 Ori C as diagnosed by the Hα emission has been very stable over the past 15 years.

The published data of Conti (1972) are potentially important for the period determination, because they extend the covered time substantially. Their published line profiles of He II λ4686 (their Fig. 2), show a blue-shifted emission appearing between JD 2 441 284.91 and 2 441 287.88. According to Stahl et al. (1996) (their Fig. 7), this emission appears at a phase of about 0.7. Together with our zero-point, this constrains the period to $15.42 < P < 15.426$, in agreement with the period obtained from Hα. Quantitative equivalent width measurements on the spectra of Conti (1972) could provide stronger constraints.

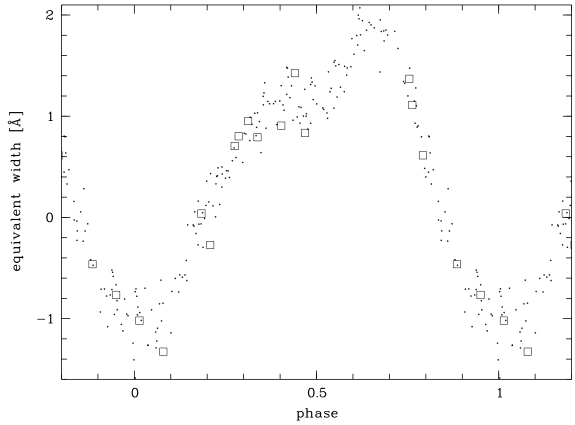

Fig. 5. The phase diagram of the equivalent width of Hα as computed with a zero point of JD = 2 448 833.0 and a period of 15.424 days. The new measurements are shown with the larger symbols.

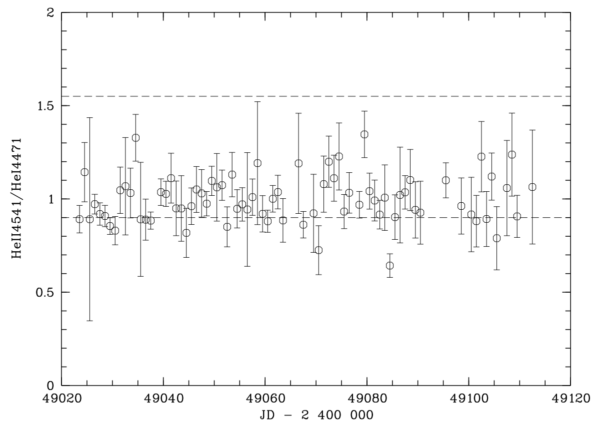

Fig. 6. The equivalent width ratio He II λ4541/He I λ4471 versus time. The horizontal lines at 0.9 and 1.55 mark the approximate ratio for the spectral types O7V and O5V, respectively. The measured ratio indicates a spectral type of about O7V.

5. Other variations

The spectacular spectral type variations, occuring on a time-span of a few days, reported by Walborn (1981) are similar to the variations reported by Walborn et al. (2003) for the other known magnetic O star, HD 191612. In the case of HD 191612, the spectral type variations are periodic with the rotational period. For θ^1 Ori C, periodic equivalent variations of HeI and HeII lines have also been reported (Stahl et al. 1996). However, the He I and He II lines vary in phase and the ratio of these lines does not vary significantly with the rotational period (Stahl et al. 1996). This behavior has been explained by Simón-Díaz et al. (2006) by variable continuum emission from a disk. The variations found by Walborn (1981) are different and thus probably had a different origin. In order to check our large data set for similar variations as reported by Walborn (1981), we searched for spectral type variations of θ^1 Ori C in our spectra. We analyzed the ratio HeII λ4541/HeI λ4471. No variations similar to those observed by Walborn (1981) were found. As an example, we show in Fig. 6 the result of our measurements in the same time interval as the measurements in Fig. 2. The measurements indicate a spectral type of about 07V, with little variation over time. For comparison, the ratios reported by Walborn (1981) lie between 1.25 and 2.11, i.e. they indicate a much earlier spectral type. We have to conclude that such spectral-type variations are rare events in θ^1 Ori C.

6. Discussion and conclusions

The long-term radial velocity variations of θ^1 Ori C are in good agreement with the orbital motion expected from the published interferometric orbit. Future radial velocity studies are very important to complete the phase coverage. Together with the interferometric data (Kraus et al. 2007; Patience et al. 2008) this should eventually provide data covering the full orbit of θ^1 Ori C. The interferometric and the radial velocity data are complementary, since some parameters are better constrained by interferometry, while others are more sensitive to radial velocity measurements.

We derive a system velocity of about 13 km s^{-1} for θ^1 Ori C, which is close to the velocity of the nebular emission, but significantly below the radial velocity of the Orion molecular cloud and the stars of the Orion nebula cluster, which have a heliocentric radial velocity of about 30 km s^{-1} (O'Dell 2001). While this discrepancy was already known from previous measurements, our result indicates that the discrepancy is not due to orbital motion. A large peculiar velocity of θ^1 Ori C would have major effects on the ionization of the Orion nebula (O'Dell 2001). However, given the peculiar spectrum of θ^1 Ori C, atmospheric effects can not be ruled out completely. At least the occasional radial velocity deviations towards smaller values (cf. Fig. 2) are probably due to atmospheric distortions and could bias the measured systemic velocity to slightly (by about 3 km s^{-1}) smaller values. In any case, the good agreement of the interferometric orbit with the radial velocity variations strongly indicates that the long-term radial-velocity variations are due to orbital motion.

According to Hillenbrand (1997), θ^1 Ori C is younger than 1 Myr. From its long period, we know that it is rotating very slowly for an O-type star. A low rotation velocity of $v \sin =$ 24 km s^{-1} has been found by direct spectroscopic analysis (Simón-Díaz et al. 2006). Assuming that θ^1 Ori C was born as a fast rotator, this suggests that strong magnetic braking must have occurred.

If it is assumed that the 538 d spectral variability period of HD 191612 (Howarth et al. 2007) is in fact the rotational period of that star (an exceptionally long period for an O star), it would appear that magnetic fields are very effective in slowing down the rotation rate. Interestingly, HD 191612 also seems to be a member of a wide binary system (Howarth et al. 2007) with an orbital period of 1542 d.

A factor of 10 decrease in rotational speed over its lifetime is plausible for θ^1 Ori C. If we assume that $p/\dot{p}$ was constant with time, this leads to an *e*-folding time of of 500 000 years or less. On the other hand, a period change of 0.001 days in 20 years corresponds to a $p/\dot{p}$ of 300 000 years. It seems therefore possible to directly measure the deceleration age of θ^1 Ori C in the foreseeable future. Equivalent width measurements, especially at phase around 0.25 and 0.75, are needed. At these phases the equivalent width changes rapidly with time, therefore observations at these phases are particularly sensitive to the exact value of the period. We have demonstrated that observations acquired using small telescopes are sufficient for this purpose.

However, in order to measure intrinsic period changes, the orbital velocity of θ^1 Ori C (which introduces a variable Doppler shift on the observed period) has to be determined with high accuracy. An orbital velocity of only 3 km s^{-1} already changes the *observed* period by 10^{-5} P, which is close to the current accuracy of the period. It is especially important to cover the minimum of the radial velocity curve. Unpublished measurements could be very valuable to fill the phase diagram. If these measurements are not available, a few more years of radial velocity monitoring are needed.

Acknowledgements. This research has made use of the SIMBAD database, operated at CDS, Strasbourg, France. G.A.W. acknowledges Discovery Grant from the Natural Science and Engineering Research Council of Canada.

References

Abt, H. A., Wang, R., & Cardona, O. 1991, ApJ, 367, 155
Babel, J., & Montmerle, T. 1997, ApJ, 485, L29
Conti, P. S. 1972, ApJ, 174, L79
Donati, J.-F., Babel, J., Harries, T. J., et al. 2002, MNRAS, 333, 55
Donati, J.-F., Howarth, I. D., Bouret, J.-C., et al. 2006, MNRAS, 365, L6
Frost, E. B., Barrett, S. B., & Struve, O. 1926, ApJ, 64, 1
Gagné, M., Caillault, J.-P., Stauffer, J. R., & Linsky, J. L. 1997, ApJ, 478, L87
Gagné, M., Oksala, M. E., Cohen, D. H., et al. 2005, ApJ, 628, 986
Hillenbrand, L. A. 1997, AJ, 113, 1733
Howarth, I. D., Walborn, N. R., Lennon, D. J., et al. 2007, MNRAS, 381, 433
Jeffries, R. D. 2007, MNRAS, 376, 1109
Kraus, S., Balega, Y. Y., Berger, J.-P., et al. 2007, A&A, 466, 649
Morrell, N., & Levato, H. 1991, ApJS, 75, 965
Moultaka, J., Ilovaisky, S. A., Prugniel, P., & Soubiran, C. 2004, PASP, 116, 693
O'Dell, C. R. 2001, ARA&A, 39, 99
Patience, J., Zavala, R. T., Prato, L., et al. 2008, ApJ, 674, L97
Petit, V., Wade, G. A., Drissen, L., Montmerle, T., & Alecian, E. 2008, MNRAS, in press
Reiners, A., Stahl, O., Wolf, B., Kaufer, A., & Rivinius, T. 2000, A&A, 363, 585
Schwarzenberg-Czerny, A. 1989, MNRAS, 241, 153
Simón-Díaz, S., Herrero, A., Esteban, C., & Najarro, F. 2006, A&A, 448, 351
Stahl, O. 1997, in ESO Workshop on Cyclic Variability in Stellar Winds, ed. L. Kaper, & A. Fullerton, 246
Stahl, O., Wolf, B., Gäng, T., et al. 1993, A&A, 274, L29
Stahl, O., Kaufer, A., Rivinius, T., et al. 1996, A&A, 312, 539
Struve, O., & Titus, J. 1944, ApJ, 99, 84
ud-Doula, A., & Owocki, S. P. 2002, ApJ, 576, 413
Vitrichenko, É. A. 2002, Astron. Lett., 28, 324
Wade, G. A., Fullerton, A. W., Donati, J.-F., et al. 2006, A&A, 451, 195
Walborn, N. R. 1981, ApJ, 243, L37
Walborn, N. R., Howarth, I. D., Herrero, A., & Lennon, D. J. 2003, ApJ, 588, 1025
Walborn, N. R., & Nichols, J. S. 1994, ApJ, 425, L29

Table 4. Radial velocity measurements.

JD - 2 400 000	C IV λ5801	C IV λ5812	He II λ5411	O III λ5592	Instrument
48 822.934	13.7 ± 1.9	3.5 ± 2.0	0.2 ± 3.3	13.8 ± 2.7	Flash
48 823.915	7.8 ± 1.7	2.3 ± 1.6	3.2 ± 2.7	11.7 ± 2.2	Flash
48 824.919	2.8 ± 1.8	1.2 ± 1.2	3.1 ± 2.1	4.2 ± 2.7	Flash
48 825.912	3.9 ± 1.8	3.2 ± 1.1	7.2 ± 1.5	7.6 ± 1.6	Flash
48 829.915	11.1 ± 2.0	7.3 ± 1.6	10.3 ± 2.4	8.1 ± 2.0	Flash
48 830.915	10.7 ± 1.9	2.8 ± 0.9	16.3 ± 1.7	9.3 ± 2.5	Flash
48 833.903	10.1 ± 1.7	8.1 ± 0.8	12.2 ± 1.7	13.7 ± 1.5	Flash
48 835.909	9.9 ± 0.9	5.5 ± 1.0	14.4 ± 1.4	8.9 ± 1.5	Flash
48 836.902	9.4 ± 0.9	6.5 ± 2.0	10.7 ± 1.6	6.9 ± 1.6	Flash
48 837.903	9.5 ± 1.4	9.6 ± 1.2	6.8 ± 1.8	9.1 ± 2.1	Flash
48 838.892	9.3 ± 0.9	4.5 ± 2.0	11.1 ± 1.3	13.8 ± 1.9	Flash
48 839.896	7.1 ± 1.1	2.0 ± 0.9	11.3 ± 1.1	9.1 ± 1.8	Flash
48 841.889	5.0 ± 0.8	6.3 ± 2.5	4.4 ± 1.3	4.4 ± 2.1	Flash
48 844.888	5.2 ± 1.0	3.3 ± 1.0	8.5 ± 1.2	6.7 ± 1.7	Flash
48 845.878	6.2 ± 0.7	5.4 ± 0.7	9.4 ± 1.2	5.6 ± 1.7	Flash
48 847.876	4.0 ± 0.6	3.3 ± 0.8	14.3 ± 1.2	8.9 ± 1.5	Flash
48 848.879	5.2 ± 0.7	3.2 ± 1.4	9.5 ± 1.4	8.7 ± 1.4	Flash
49 023.551	13.9 ± 0.8	9.3 ± 2.1	16.3 ± 1.2	9.3 ± 1.5	Flash
49 024.535	10.4 ± 0.9	14.0 ± 1.1	10.3 ± 1.7	10.9 ± 2.3	Flash
49 025.551	9.7 ± 0.8	9.1 ± 2.0	6.8 ± 1.7	6.5 ± 1.9	Flash
49 026.535	8.9 ± 0.8	7.6 ± 1.0	10.1 ± 1.1	10.9 ± 1.3	Flash
49 027.543	10.8 ± 0.7	6.2 ± 1.1	13.3 ± 1.5	9.8 ± 1.5	Flash
49 028.543	11.0 ± 0.8	7.3 ± 0.7	8.9 ± 1.3	7.8 ± 1.6	Flash
49 029.535	9.5 ± 1.7	7.9 ± 2.1	12.5 ± 1.3	6.6 ± 1.0	Flash
49 030.543	12.2 ± 0.7	7.7 ± 0.8	15.2 ± 1.6	5.7 ± 1.1	Flash
49 031.539	11.2 ± 0.8	8.4 ± 0.7	13.7 ± 1.3	8.1 ± 0.9	Flash
49 032.562	8.7 ± 0.6	7.1 ± 0.6	14.4 ± 1.3	6.2 ± 2.0	Flash
49 033.555	9.5 ± 1.6	6.6 ± 1.3	15.8 ± 1.9	11.2 ± 1.3	Flash
49 034.578	9.9 ± 0.6	9.7 ± 0.7	16.0 ± 1.3	10.3 ± 2.1	Flash
49 035.547	9.0 ± 0.7	10.0 ± 0.8	12.7 ± 1.5	10.1 ± 1.2	Flash
49 036.543	8.1 ± 0.7	6.8 ± 1.0	6.4 ± 1.5	10.0 ± 0.8	Flash
49 037.535	7.8 ± 0.8	4.2 ± 1.0	3.3 ± 1.7	7.7 ± 1.3	Flash
49 038.609	8.2 ± 1.6	−0.9 ± 2.0	2.4 ± 3.7	10.7 ± 2.1	Flash
49 039.539	5.7 ± 0.7	2.8 ± 1.0	9.9 ± 1.2	6.8 ± 2.2	Flash
49 040.523	1.8 ± 0.8	−2.6 ± 1.4	5.4 ± 1.4	5.1 ± 1.3	Flash
49 041.527	4.2 ± 0.9	−0.4 ± 1.0	−5.0 ± 1.6	1.4 ± 1.4	Flash
49 042.527	0.1 ± 1.0	−2.5 ± 0.7	2.5 ± 1.7	. .	Flash
49 043.535	1.2 ± 0.7	−3.1 ± 0.8	5.8 ± 1.8	−3.2 ± 1.3	Flash
49 044.535	0.7 ± 0.7	−3.1 ± 0.6	2.7 ± 1.4	−1.2 ± 1.1	Flash
49 045.527	3.0 ± 0.6	−0.5 ± 0.6	8.3 ± 1.0	0.4 ± 1.1	Flash
49 046.523	3.1 ± 0.7	2.1 ± 1.0	9.3 ± 1.5	3.3 ± 1.3	Flash
49 047.527	3.9 ± 0.7	0.1 ± 0.6	11.9 ± 1.3	2.0 ± 1.1	Flash
49 048.523	4.6 ± 0.7	4.2 ± 0.7	12.7 ± 1.3	4.6 ± 0.9	Flash
49 049.520	7.4 ± 0.8	5.1 ± 0.9	14.1 ± 1.2	7.6 ± 1.0	Flash
49 050.523	10.4 ± 0.7	8.6 ± 0.8	14.9 ± 1.5	11.0 ± 1.1	Flash
49 051.547	11.0 ± 0.8	8.5 ± 0.8	10.9 ± 1.3	9.2 ± 1.1	Flash
49 052.547	11.2 ± 1.6	7.0 ± 0.8	14.8 ± 1.7	9.3 ± 1.3	Flash
49 053.523	12.1 ± 0.8	7.8 ± 1.0	13.4 ± 2.3	8.4 ± 1.3	Flash
49 054.512	13.1 ± 1.0	7.9 ± 0.9	11.6 ± 1.3	15.1 ± 1.2	Flash
49 055.516	11.8 ± 1.0	10.6 ± 1.2	12.2 ± 1.5	7.2 ± 1.3	Flash
49 056.512	11.6 ± 1.0	8.4 ± 1.0	12.3 ± 1.4	7.6 ± 1.4	Flash
49 057.520	10.0 ± 1.2	7.2 ± 0.9	11.6 ± 1.2	12.2 ± 1.2	Flash
49 058.512	12.8 ± 0.8	8.3 ± 1.0	11.6 ± 1.2	15.2 ± 2.6	Flash
49 059.512	11.5 ± 0.7	10.7 ± 0.9	12.9 ± 1.3	15.9 ± 1.5	Flash
49 060.516	14.9 ± 0.8	10.7 ± 0.9	16.0 ± 2.2	10.5 ± 2.5	Flash
49 061.512	16.0 ± 0.8	5.2 ± 1.0	19.8 ± 1.2	10.2 ± 1.0	Flash
49 062.512	13.4 ± 0.7	11.2 ± 0.8	19.1 ± 1.5	14.2 ± 1.1	Flash
49 063.516	13.2 ± 0.7	12.4 ± 0.7	19.7 ± 1.3	13.2 ± 1.8	Flash
49 065.512	16.1 ± 0.7	14.6 ± 0.8	19.4 ± 1.3	17.3 ± 1.3	Flash
49 066.578	15.8 ± 1.0	12.9 ± 1.3	16.4 ± 2.7	16.3 ± 2.1	Flash
49 067.512	14.4 ± 0.6	13.3 ± 0.8	17.9 ± 1.3	14.6 ± 1.1	Flash
49 068.512	15.5 ± 0.8	12.8 ± 1.1	15.1 ± 1.4	14.6 ± 1.8	Flash
49 069.516	16.5 ± 1.2	12.6 ± 1.3	23.3 ± 4.8	19.3 ± 1.9	Flash
49 070.516	15.7 ± 1.0	12.6 ± 0.8	15.8 ± 1.7	12.5 ± 1.3	Flash

Table 4. continued.

JD - 2 400 000	C IV λ5801	C IV λ5812	He II λ5411	O III λ5592	Instrument
49 071.516	13.6 ± 1.1	9.8 ± 0.9	17.6 ± 1.6	14.8 ± 1.3	Flash
49 072.516	12.6 ± 1.1	10.3 ± 1.2	17.6 ± 1.5	16.8 ± 3.0	Flash
49 073.527	14.2 ± 0.9	12.9 ± 0.7	15.6 ± 1.3	9.6 ± 1.4	Flash
49 074.520	14.4 ± 0.8	13.4 ± 0.8	15.7 ± 1.3	11.6 ± 2.0	Flash
49 075.520	15.1 ± 0.7	8.6 ± 1.1	17.5 ± 1.2	8.1 ± 4.4	Flash
49 076.516	15.5 ± 0.9	11.4 ± 0.9	15.3 ± 1.6	11.9 ± 1.2	Flash
49 078.520	15.9 ± 0.7	13.6 ± 0.7	21.6 ± 1.3	13.1 ± 1.2	Flash
49 079.516	15.1 ± 0.7	12.7 ± 1.8	22.0 ± 1.3	14.9 ± 1.0	Flash
49 080.512	15.0 ± 0.6	13.4 ± 0.7	21.1 ± 1.3	15.3 ± 1.4	Flash
49 081.520	16.1 ± 0.7	14.4 ± 0.7	22.8 ± 1.4	16.8 ± 1.2	Flash
49 082.516	15.1 ± 0.7	14.1 ± 1.3	16.3 ± 1.4	12.8 ± 1.2	Flash
49 083.508	12.8 ± 1.2	14.6 ± 1.2	17.3 ± 1.7	13.0 ± 1.7	Flash
49 084.504	19.3 ± 1.9	12.1 ± 0.8	9.3 ± 1.3	14.7 ± 1.2	Flash
49 085.508	19.5 ± 1.2	11.0 ± 1.0	14.3 ± 1.3	17.4 ± 1.6	Flash
49 086.504	11.3 ± 1.2	11.7 ± 1.0	9.5 ± 1.5	15.6 ± 1.3	Flash
49 087.500	11.2 ± 1.6	8.2 ± 0.8	5.0 ± 1.2	16.7 ± 2.6	Flash
49 088.508	11.4 ± 1.2	7.0 ± 0.8	14.3 ± 1.6	14.6 ± 1.7	Flash
49 089.520	13.3 ± 1.2	9.6 ± 0.9	13.1 ± 1.7	10.9 ± 2.7	Flash
49 090.504	13.5 ± 1.2	9.7 ± 0.9	11.7 ± 1.3	9.1 ± 4.2	Flash
49 095.504	14.1 ± 0.7	11.8 ± 1.3	14.6 ± 1.4	17.7 ± 2.2	Flash
49 098.539	7.4 ± 1.1	6.8 ± 1.2	11.4 ± 2.0	8.3 ± 1.5	Flash
49 100.504	4.0 ± 1.5	3.3 ± 1.0	11.2 ± 1.3	7.8 ± 1.0	Flash
49 101.504	6.4 ± 1.0	3.5 ± 1.3	7.8 ± 1.4	6.8 ± 1.1	Flash
49 102.496	2.3 ± 1.2	0.6 ± 0.9	7.4 ± 1.1	4.0 ± 1.4	Flash
49 103.496	0.3 ± 0.9	1.4 ± 0.8	7.1 ± 1.7	1.9 ± 1.0	Flash
49 104.508	0.7 ± 1.1	−2.0 ± 1.0	7.7 ± 1.1	0.1 ± 1.1	Flash
49 105.504	−2.0 ± 2.7	−2.0 ± 2.8	0.0 ± 3.8	2.3 ± 2.2	Flash
49 107.496	4.0 ± 0.6	0.8 ± 1.1	13.7 ± 1.6	1.8 ± 1.6	Flash
49 108.492	7.7 ± 1.4	3.6 ± 1.3	16.2 ± 1.7	4.8 ± 1.4	Flash
49 109.504	4.2 ± 0.9	2.3 ± 0.8	9.2 ± 1.5	6.5 ± 2.3	Flash
49 112.508	14.1 ± 1.1	10.0 ± 1.2	16.4 ± 2.0	12.4 ± 1.4	Flash
49 387.544	18.3 ± 0.8	14.2 ± 0.7	25.7 ± 1.2	16.4 ± 1.2	Flash
49 392.566	17.2 ± 0.8	15.9 ± 0.9	17.8 ± 1.5	16.5 ± 1.5	Flash
49 395.539	14.8 ± 2.7	13.8 ± 3.0	20.3 ± 1.8	15.9 ± 2.4	Flash
49 401.526	16.9 ± 0.7	15.4 ± 0.9	22.1 ± 1.2	13.7 ± 1.3	Flash
49 406.519	11.9 ± 0.7	10.1 ± 0.8	13.6 ± 1.5	12.6 ± 1.0	Flash
49 413.517	5.0 ± 0.9	0.4 ± 0.8	7.3 ± 1.4	7.2 ± 1.2	Flash
49 422.549	17.3 ± 0.8	15.9 ± 0.8	19.0 ± 1.5	18.0 ± 1.8	Flash
49 429.517	16.5 ± 0.7	15.3 ± 1.2	18.2 ± 1.3	18.8 ± 9.2	Flash
49 433.520	19.1 ± 0.7	11.5 ± 1.8	22.2 ± 1.1	15.4 ± 1.4	Flash
49 759.567	. .	. .	25.8 ± 1.8	. .	Heros
49 771.591	. .	. .	23.6 ± 2.1	. .	Heros
49 776.570	. .	. .	17.0 ± 1.7	. .	Heros
49 777.574	. .	. .	14.3 ± 1.7	. .	Heros
49 778.519	. .	. .	15.5 ± 1.5	. .	Heros
49 779.518	. .	. .	6.3 ± 2.0	. .	Heros
49 780.518	. .	. .	9.9 ± 1.5	. .	Heros
49 781.517	. .	. .	3.2 ± 2.3	. .	Heros
49 782.520	. .	. .	6.4 ± 1.6	. .	Heros
49 783.517	. .	. .	5.8 ± 2.2	. .	Heros
49 784.517	. .	. .	−6.3 ± 2.9	. .	Heros
49 785.517	. .	. .	16.4 ± 2.1	. .	Heros
49 786.520	. .	. .	15.3 ± 2.0	. .	Heros
49 787.543	. .	. .	23.3 ± 2.1	. .	Heros
49 788.522	. .	. .	16.6 ± 1.9	. .	Heros
49 789.519	. .	. .	16.0 ± 1.8	. .	Heros
49 790.505	. .	. .	24.0 ± 2.0	. .	Heros
49 791.545	. .	. .	21.9 ± 2.5	. .	Heros
49 792.518	. .	. .	21.0 ± 2.1	. .	Heros
49 793.510	. .	. .	20.5 ± 3.8	. .	Heros
49 794.506	. .	. .	22.1 ± 1.5	. .	Heros
49 795.509	. .	. .	18.2 ± 5.6	. .	Heros
49 796.503	. .	. .	25.1 ± 1.7	. .	Heros
49 797.506	. .	. .	17.8 ± 1.7	. .	Heros
49 798.499	. .	. .	16.7 ± 1.7	. .	Heros
50 030.595	14.4 ± 0.3	11.2 ± 0.3	16.2 ± 0.7	13.2 ± 0.5	Elodie

Table 4. continued.

JD - 2 400 000	C IV λ5801	C IV λ5812	He II λ5411	O III λ5592	Instrument
50 716.651	. .	. .	43.6 ± 2.2	27.5 ± 2.0	Heros
50 717.618	. .	. .	33.9 ± 1.7	29.3 ± 2.3	Heros
50 718.590	. .	. .	30.9 ± 1.9	32.3 ± 1.7	Heros
50 719.612	. .	. .	30.2 ± 1.7	30.9 ± 2.0	Heros
50 726.583	31.7 ± 1.6	23.9 ± 1.2	30.7 ± 2.4	24.8 ± 2.4	Heros
50 727.597	27.2 ± 1.0	26.1 ± 1.2	. .	. .	Heros
51 097.892	34.7 ± 0.3	32.2 ± 0.3	37.9 ± 0.5	19.1 ± 3.7	Feros
51 134.880	23.3 ± 0.2	20.7 ± 0.3	24.1 ± 0.5	20.6 ± 0.5	Feros
51 145.866	32.1 ± 0.3	28.7 ± 0.2	38.3 ± 0.5	30.6 ± 0.5	Feros
51 148.801	35.1 ± 0.3	32.0 ± 0.2	38.1 ± 0.5	33.3 ± 0.5	Feros
51 151.776	34.7 ± 0.4	31.8 ± 0.3	34.3 ± 0.6	33.6 ± 0.6	Feros
51 172.579	34.4 ± 0.5	28.1 ± 0.6	34.6 ± 0.7	30.6 ± 1.1	Feros
51 177.579	34.4 ± 0.3	32.2 ± 0.3	40.5 ± 0.7	34.1 ± 0.6	Feros
51 179.593	34.0 ± 0.3	31.3 ± 0.3	38.4 ± 0.6	33.8 ± 0.6	Feros
51 180.513	33.5 ± 0.4	31.4 ± 0.3	35.5 ± 0.8	11.5 ± 6.5	Feros
51 191.700	26.0 ± 0.2	22.4 ± 0.2	0.5 ± 0.5	23.5 ± 0.5	Feros
51 192.551	24.5 ± 0.2	22.2 ± 0.2	31.5 ± 0.5	22.7 ± 0.6	Feros
51 373.931	32.5 ± 0.4	29.3 ± 0.4	35.6 ± 0.6	17.9 ± 2.2	Feros
51 380.936	25.2 ± 0.3	24.5 ± 0.3	27.8 ± 0.6	22.1 ± 0.7	Feros
51 381.937	25.9 ± 0.3	23.6 ± 0.3	27.4 ± 0.6	18.4 ± 1.5	Feros
51 382.939	26.1 ± 0.4	23.2 ± 0.4	26.0 ± 0.6	22.9 ± 0.9	Feros
51 383.932	28.4 ± 0.4	24.9 ± 0.4	25.8 ± 0.5	24.9 ± 0.6	Feros
51 384.928	28.0 ± 0.4	24.3 ± 0.4	26.0 ± 0.5	25.8 ± 0.7	Feros
51 385.935	28.3 ± 0.4	26.2 ± 0.3	29.1 ± 0.6	24.8 ± 0.9	Feros
51 386.946	29.2 ± 0.3	27.2 ± 0.3	30.2 ± 0.5	23.6 ± 0.8	Feros
51 389.933	33.7 ± 0.3	30.4 ± 0.3	36.4 ± 0.5	28.7 ± 0.4	Feros
51 390.954	34.8 ± 0.3	31.6 ± 0.2	38.7 ± 0.6	28.8 ± 0.5	Feros
51 391.947	35.6 ± 0.3	33.0 ± 0.3	41.1 ± 0.5	31.7 ± 0.5	Feros
51 392.900	35.3 ± 0.3	33.4 ± 0.3	2.1 ± 0.5	32.1 ± 0.5	Feros
51 393.950	37.5 ± 0.3	34.9 ± 0.2	43.5 ± 0.5	29.8 ± 1.3	Feros
51 394.935	37.9 ± 0.3	35.2 ± 0.3	43.1 ± 0.5	34.2 ± 0.7	Feros
53 329.563	11.6 ± 0.8	9.3 ± 1.4	15.6 ± 0.9	11.2 ± 0.7	Elodie
53 740.534	21.6 ± 0.2	18.5 ± 0.4	21.6 ± 0.9	21.4 ± 0.6	Feros
51 578.422	37.8 ± 0.7	35.3 ± 0.5	39.3 ± 1.1	36.0 ± 0.9	Musicos
51 578.454	36.9 ± 0.7	35.2 ± 0.6	37.3 ± 1.2	37.5 ± 0.7	Musicos
51 579.393	40.1 ± 0.8	37.9 ± 0.5	38.2 ± 1.1	38.5 ± 0.7	Musicos
51 579.423	39.9 ± 0.6	36.6 ± 0.5	40.1 ± 1.1	39.1 ± 0.7	Musicos
51 579.454	38.4 ± 0.6	36.9 ± 0.5	40.3 ± 1.1	37.5 ± 0.6	Musicos
51 587.374	37.6 ± 0.7	35.9 ± 0.6	34.2 ± 1.2	38.7 ± 0.9	Musicos
51 590.382	39.4 ± 0.7	35.8 ± 2.6	33.3 ± 1.1	37.4 ± 0.9	Musicos
51 590.413	39.0 ± 0.7	35.5 ± 7.7	33.0 ± 1.2	37.5 ± 0.9	Musicos
51 596.391	41.0 ± 0.6	37.2 ± 0.6	37.0 ± 1.2	39.2 ± 0.6	Musicos
51 596.421	40.2 ± 0.6	37.6 ± 0.5	38.3 ± 1.1	40.2 ± 0.6	Musicos
51 596.452	40.3 ± 0.6	37.6 ± 0.6	37.9 ± 1.2	40.3 ± 0.6	Musicos
51 597.351	41.2 ± 0.6	38.0 ± 0.5	36.6 ± 1.3	38.8 ± 0.6	Musicos
51 597.382	41.9 ± 0.6	37.9 ± 0.5	36.4 ± 1.2	39.6 ± 0.7	Musicos
51 597.413	41.3 ± 0.7	38.3 ± 0.5	35.5 ± 1.2	40.8 ± 0.7	Musicos
51 597.444	41.9 ± 0.7	37.7 ± 0.5	35.1 ± 1.3	39.9 ± 0.7	Musicos
51 599.353	41.4 ± 0.8	35.4 ± 0.7	32.0 ± 1.2	38.7 ± 0.6	Musicos
51 599.384	41.2 ± 0.7	35.3 ± 0.7	31.0 ± 1.4	38.6 ± 1.0	Musicos
51 599.416	40.6 ± 0.7	34.6 ± 0.7	27.7 ± 1.4	39.3 ± 1.1	Musicos
51 600.346	40.0 ± 0.8	35.7 ± 2.8	32.2 ± 1.1	39.6 ± 1.2	Musicos
51 600.378	40.2 ± 0.8	36.7 ± 0.9	33.7 ± 1.2	38.5 ± 1.3	Musicos
51 600.410	38.7 ± 0.8	36.1 ± 5.6	31.0 ± 1.2	37.5 ± 0.9	Musicos
51 601.361	38.8 ± 0.8	34.6 ± 0.8	30.6 ± 1.2	38.8 ± 1.2	Musicos
51 601.392	39.3 ± 0.8	34.8 ± 0.8	31.8 ± 1.2	39.1 ± 1.3	Musicos
51 601.423	38.3 ± 0.7	33.4 ± 1.1	29.0 ± 1.2	36.6 ± 1.2	Musicos
51 602.349	37.8 ± 0.7	34.4 ± 0.6	31.6 ± 1.1	38.9 ± 1.2	Musicos
51 602.388	38.4 ± 0.6	34.6 ± 0.5	31.0 ± 1.1	37.2 ± 0.9	Musicos
51 602.419	38.2 ± 0.6	35.0 ± 0.7	30.9 ± 1.2	39.1 ± 1.1	Musicos
51 603.377	38.3 ± 0.7	35.7 ± 4.0	31.7 ± 1.3	39.1 ± 1.1	Musicos
51 603.408	38.9 ± 0.7	36.2 ± 2.9	34.1 ± 1.2	39.5 ± 1.2	Musicos
51 603.439	38.2 ± 0.8	34.9 ± 6.2	29.2 ± 1.4	38.3 ± 1.2	Musicos
51 606.353	38.6 ± 0.7	36.5 ± 5.2	37.4 ± 1.1	36.4 ± 0.8	Musicos

Table 4. continued.

JD - 2 400 000	C IV λ5801	C IV λ5812	He II λ5411	O III λ5592	Instrument
51 606.384	40.9 ± 0.7	37.4 ± 10.2	38.1 ± 1.0	36.5 ± 0.8	Musicos
51 606.416	39.7 ± 0.7	36.2 ± 3.7	37.2 ± 1.1	37.2 ± 1.0	Musicos
51 608.370	37.4 ± 0.6	35.7 ± 0.5	40.0 ± 1.1	36.7 ± 0.4	Musicos
51 608.401	38.3 ± 0.7	36.0 ± 0.5	40.5 ± 1.1	37.0 ± 0.5	Musicos
51 608.431	38.3 ± 0.6	36.3 ± 0.6	39.0 ± 1.2	36.3 ± 0.6	Musicos
51 609.361	39.3 ± 0.6	36.2 ± 0.6	38.3 ± 1.7	39.1 ± 0.6	Musicos
51 609.391	38.4 ± 0.6	36.4 ± 0.5	39.7 ± 1.1	37.5 ± 0.6	Musicos
51 609.422	39.7 ± 0.7	36.4 ± 0.7	36.5 ± 1.2	39.0 ± 0.6	Musicos
53 744.891	20.1 ± 0.2	17.0 ± 0.2	21.3 ± 0.5	18.2 ± 0.4	Espadons
54 169.854	26.0 ± 0.2	23.1 ± 0.2	32.2 ± 0.5	23.4 ± 0.4	Espadons
54 456.748	15.4 ± 0.2	11.9 ± 0.2	16.9 ± 0.4	12.9 ± 0.3	Espadons
54 457.748	17.1 ± 0.2	13.8 ± 0.2	19.5 ± 0.5	13.6 ± 0.2	Espadons

Table 5. Equivalent width measurements.

JD − 2 400 000	Hα	He II λ4686	instrument
48 822.934	0.640	0.309	Flash
48 823.915	1.059	0.202	Flash
48 824.919	0.873	0.195	Flash
48 825.912	1.276	0.361	Flash
48 829.915	0.400	0.131	Flash
48 830.915	−0.134	0.033	Flash
48 833.903	−1.133	−0.140	Flash
48 835.909	−0.296	−0.032	Flash
48 836.902	0.462	0.136	Flash
48 837.903	0.990	0.258	Flash
48 838.892	1.124	0.238	Flash
48 839.896	0.994	0.258	Flash
48 841.889	1.243	0.247	Flash
48 844.888	0.931	0.231	Flash
48 845.878	−0.026	0.182	Flash
48 847.876	−1.057	0.016	Flash
48 848.879	−0.700	0.196	Flash
49 023.551	1.113	0.214	Flash
49 024.535	1.216	0.195	Flash
49 025.551	0.931	−0.005	Flash
49 026.535	1.080	0.237	Flash
49 027.543	1.704	0.334	Flash
49 028.543	1.838	0.347	Flash
49 029.535	1.325	0.324	Flash
49 030.543	0.447	0.065	Flash
49 031.539	−0.062	−0.013	Flash
49 032.562	−0.713	−0.007	Flash
49 033.555	−1.587	−0.080	Flash
49 034.578	−0.853	−0.021	Flash
49 035.547	−0.591	0.185	Flash
49 036.543	0.119	0.068	Flash
49 037.535	0.395	0.152	Flash
49 038.609	1.029	0.295	Flash
49 039.539	0.918	0.181	Flash
49 040.523	0.932	0.411	Flash
49 041.527	1.068	0.080	Flash
49 042.527	1.476	0.410	Flash
49 043.535	1.903	0.278	Flash
49 044.535	1.838	0.321	Flash
49 045.527	0.906	0.375	Flash
49 046.523	−0.133	0.119	Flash
49 047.527	−0.710	−0.050	Flash
49 048.523	−0.807	−0.155	Flash
49 049.520	−1.262	−0.028	Flash
49 050.523	−0.731	0.198	Flash
49 051.547	−0.159	0.130	Flash
49 052.547	0.128	0.124	Flash
49 053.523	0.543	0.320	Flash
49 054.512	0.881	0.271	Flash
49 055.516	1.184	0.223	Flash
49 056.512	1.164	0.360	Flash
49 057.520	1.189	0.232	Flash
49 058.512	1.804	0.073	Flash
49 059.512	1.744	0.437	Flash
49 060.516	1.201	0.360	Flash
49 061.512	0.330	0.069	Flash
49 062.512	−0.417	−0.018	Flash
49 063.516	−0.959	−0.159	Flash
49 065.512	−1.023	0.069	Flash
49 066.578	−0.623	0.060	Flash
49 067.512	0.153	0.243	Flash
49 068.512	0.561	0.115	Flash
49 069.516	0.808	0.204	Flash
49 070.516	1.151	0.173	Flash
49 071.516	1.002	0.255	Flash
49 072.516	1.033	0.245	Flash

Table 5. continued.

JD − 2 400 000	Hα	He II λ4686	instrument
49 073.527	1.489	0.415	Flash
49 074.520	1.874	0.523	Flash
49 075.520	1.670	0.401	Flash
49 076.516	0.798	0.214	Flash
49 078.520	−0.707	−0.138	Flash
49 079.516	−0.971	−0.036	Flash
49 080.512	−0.912	0.014	Flash
49 081.520	−0.603	0.081	Flash
49 082.516	−0.067	0.071	Flash
49 083.508	0.429	0.246	Flash
49 084.504	0.825	0.023	Flash
49 085.508	1.124	0.353	Flash
49 086.504	0.960	0.034	Flash
49 087.500	1.122	0.273	Flash
49 088.508	1.287	0.391	Flash
49 089.520	1.648	0.365	Flash
49 090.504	1.803	0.331	Flash
49 095.504	−1.018	−0.115	Flash
49 098.539	0.115	0.124	Flash
49 100.504	0.947	0.232	Flash
49 101.504	1.112	0.299	Flash
49 102.496	1.024	0.386	Flash
49 103.496	1.242	0.341	Flash
49 104.508	1.612	0.477	Flash
49 105.504	.	0.472	Flash
49 107.496	0.485	0.056	Flash
49 108.492	0.284	0.156	Flash
49 109.504	−1.079	−0.215	Flash
49 112.508	−0.737	0.197	Flash
49 387.544	−0.912	−0.093	Flash
49 392.566	0.592	0.136	Flash
49 395.539	1.000	0.215	Flash
49 401.526	−0.235	−0.009	Flash
49 406.519	−0.063	0.055	Flash
49 413.517	1.850	0.385	Flash
49 422.549	0.007	0.097	Flash
49 429.517	1.437	0.386	Flash
49 433.520	−0.766	−0.120	Flash
49 759.566	−0.620	0.012	Heros
49 771.591	0.055	−0.034	Heros
49 776.570	0.161	0.037	Heros
49 777.574	0.499	0.123	Heros
49 778.519	0.831	0.132	Heros
49 779.518	1.146	0.146	Heros
49 780.518	1.301	0.223	Heros
49 781.517	1.300	0.160	Heros
49 782.520	1.511	0.243	Heros
49 783.517	1.945	0.270	Heros
49 784.517	1.851	0.305	Heros
49 785.517	1.475	0.272	Heros
49 786.520	0.472	0.021	Heros
49 787.543	−0.473	−0.109	Heros
49 788.522	−0.665	−0.210	Heros
49 789.518	−0.940	−0.035	Heros
49 790.505	−0.848	−0.156	Heros
49 791.545	−0.074	0.025	Heros
49 792.518	0.433	0.056	Heros
49 793.510	0.687	0.090	Heros
49 794.506	1.034	0.099	Heros
49 795.509	1.302	−0.020	Heros
49 796.502	1.266	0.125	Heros
49 797.505	1.439	0.205	Heros
49 798.498	1.767	0.244	Heros
50 030.595	1.927	0.417	Elodie
50 716.650	−0.568	0.157	Heros
50 717.617	0.047	0.154	Heros

Table 5. continued.

JD − 2 400 000	Hα	HeII λ4686	instrument
50 718.589	0.388	0.192	Heros
50 719.612	0.760	0.256	Heros
50 726.583	1.150	0.298	Heros
50 727.597	0.158	.	Heros
51 097.892	−0.034	0.051	Feros
51 134.880	0.300	0.131	Feros
51 145.866	−0.823	−0.077	Feros
51 148.801	−0.425	0.103	Feros
51 151.776	0.891	0.228	Feros
51 172.579	1.843	0.374	Feros
51 177.579	−0.963	−0.018	Feros
51 179.593	−0.568	0.099	Feros
51 180.513	0.358	0.145	Feros
51 191.700	−0.777	−0.053	Feros
51 192.551	−0.956	−0.049	Feros
51 373.931	1.343	0.401	Feros
51 380.936	−0.011	0.150	Feros
51 381.937	0.459	0.188	Feros
51 382.939	0.920	0.184	Feros
51 383.932	1.147	0.249	Feros
51 384.928	1.094	0.236	Feros
51 385.935	1.083	0.191	Feros
51 386.946	1.406	0.318	Feros
51 389.933	0.892	0.295	Feros
51 390.954	−0.227	0.050	Feros
51 391.947	−0.934	−0.083	Feros
51 392.900	−1.120	−0.073	Feros
51 393.950	−1.265	−0.007	Feros
51 394.935	−1.140	0.023	Feros
53 329.563	0.979	0.225	Elodie
51 578.422	−1.242	−0.103	Musicos
51 578.454	−1.407	−0.135	Musicos
51 579.393	−1.289	−0.061	Musicos
51 579.424	−1.222	−0.056	Musicos
51 579.454	−1.095	−0.041	Musicos
51 587.374	1.493	0.205	Musicos
51 590.382	1.280	0.243	Musicos
51 590.413	1.103	0.249	Musicos
51 596.391	−0.074	0.177	Musicos
51 596.421	−0.086	0.123	Musicos
51 596.452	0.056	0.136	Musicos
51 597.351	0.332	0.161	Musicos
51 597.382	0.405	0.193	Musicos
51 597.413	0.412	0.190	Musicos
51 597.444	0.490	0.168	Musicos
51 599.353	1.196	0.219	Musicos
51 599.384	1.230	0.216	Musicos
51 599.416	1.331	0.214	Musicos
51 600.346	1.483	0.247	Musicos
51 600.378	1.474	0.223	Musicos
51 600.411	1.386	0.236	Musicos
51 601.361	1.313	0.220	Musicos
51 601.392	1.379	0.209	Musicos
51 601.423	1.337	0.219	Musicos
51 602.349	1.534	0.275	Musicos
51 602.388	1.551	0.266	Musicos
51 602.419	1.498	0.247	Musicos
51 603.377	2.000	0.316	Musicos
51 603.408	1.964	0.322	Musicos
51 603.439	2.072	0.283	Musicos
51 606.353	0.803	0.258	Musicos
51 606.384	0.797	0.211	Musicos
51 606.416	0.637	0.224	Musicos
51 608.370	−0.521	0.057	Musicos
51 608.400	−0.542	0.033	Musicos
51 608.431	−0.583	0.012	Musicos

Table 5. continued.

JD − 2 400 000	Hα	HeII λ4686	instrument
51 609.360	−0.734	0.121	Musicos
51 609.391	−0.705	0.130	Musicos
51 609.422	−0.779	0.198	Musicos
53 740.534	−0.271	0.157	Feros
53 744.891	1.087	0.215	Espadons
54 169.854	−0.886	0.004	Espadons
54 456.748	1.798	0.389	Espadons
54 457.748	1.952	0.454	Espadons
54 505.248	1.370	.	Lhires III,1
54 505.375	1.110	.	Lhires III,3
54 507.262	−0.462	.	Lhires III,1
54 508.264	−0.765	.	Lhires III,1
54 509.248	−1.02	.	Lhires III,1
54 510.259	−1.327	.	Lhires III,1
54 512.244	−0.273	.	Lhires III,1
54 513.28	0.706	.	Lhires III,1
54 514.245	0.792	.	Lhires III,1
54 515.253	0.907	.	Lhires III,1
54 516.257	0.836	.	Lhires III,1
54 521.248	0.614	.	Lhires III,1
54 527.294	0.039	.	Lhires III,2
54 529.272	0.952	.	Lhires III,2
54 531.252	1.426	.	Lhires III,2
54 544.297	0.802	.	Lhires III.2